Performance Testing and Evaluation of a High Temperature Xenon Resistojet Prototype Manufactured by Selective Laser Melting

IEPC-2017-463

Presented at the 35th International Electric Propulsion Conference
Georgia Institute of Technology • Atlanta, Georgia • USA
October 8 – 12, 2017

Federico Romei[1] and Angelo Grubišić[2]
University of Southampton, Southampton, SO17 1BJ, UK

Dave Gibbon [3]
Surrey Satellite Technology Ltd, Guildford, GU2 7YE, UK

Abstract: This paper presents performance testing and evaluation of the AMR-X-0, the first additively manufactured breadboard model resistojet thruster with a novel design of heat exchanger. Testing is performed within the David Fearn Electric Propulsion Laboratory at the University of Southampton. The thruster is characterized at constant flow rates with argon, in both cold gas mode and at a range of electrical power inputs with current regulation. Thrust measurements demonstrate an improvement in ISP of 50% and thus validating the concept and providing insight into the thermal inertia of the AMR-X thruster. The presence of a gas leak caused by a ceramic component is discussed.

I. Introduction

Electrothermal propulsion systems for spacecraft consist of an electrically powered heat exchanger, which increases the enthalpy of a propellant. Enthalpy is traded for kinetic energy through a gas dynamic expansion process to produce a high velocity exhaust jet via a converging-diverging nozzle producing thrust. The performance is quantified by the specific impulse (ISP), which increases proportionally to the square root of the stagnation gas temperature, Eq.(1). By increasing the stagnation temperature, the amount of propellant required on board of the spacecraft to accomplish a specific mission decreases or greater total impulse is provided for a fixed quantity of propellant.

Surrey Satellite Technology Limited (SSTL) has used a low power hot gas system, known as a resistojet, since 2002, which uses either butane or xenon as propellant. This system has flown on 20 spacecraft including the European GPS Galileo Testbed GIOVE-A validation satellite[1-3]. This low cost and relatively low temperature resistojet significantly improves the performance of the traditional cold gas propulsion systems. A collaborative development programme between the University of Southampton and SSTL is currently underway to develop a High Temperature Xenon Resistojet (HTXR), which nearly doubles current ISP performance. Selective Laser Melting (SLM) manufacturing is being utilized to build a novel complex thin-wall concentric tubular heat exchanger as a single

[1] PhD Candidate, Astronautics Research Group, f.romei@soton.ac.uk
[2] Lecturer, Astronautics Research Group, a.grubisic@soton.ac.uk
[3] Propulsion Expert, d.gibbon@sstl.co.uk

component, and is termed the Additively Manufactured Resistojet with Xenon (AMR-X). The AMR-X is designed to increase the stagnation temperature of the propellant to approximately 3,000 K. The theoretical total thruster efficiency obtained from multiphysics models is in the range of 65-90% and, depending on the thrust level, the resulting ISP for xenon propellant is above 80s. This research programme includes design, multiphysics modelling, manufacturing, performance testing and ultimately the validation of an engineering model thruster.

Presently, the primary driver of resistojet technology is a requirement for the all-electric propulsion spacecraft bus[4]. Geostationary telecommunication satellites typically use chemical propulsion for attitude control as well as orbit–raising and station-keeping. The benefit of using an AMR-X is in fuel load reduction, cost savings in launch vehicle option for lighter spacecraft and further reduction of integration and testing costs by eliminating the use of hazardous propellants. A second driver of the resistojet technology is the small Low Earth Orbit (LEO) platform. These satellites have limited resources, such as low volume and power budgets, therefore, they depend upon high density ISP (propellant storage density – ISP product), and rely on inert propellants to lower assembly integration and testing (AIT) costs. The resulting propulsion system has low ISP, low total impulse and therefore limited on-orbit/deorbit capability. As a result, a low power AMR-X would meet both of these applications.

II. Design and Test Method

The AMR-X heat exchanger and nozzle are integrated in a complex thin-wall concentric tubular single component additively manufactured by SLM. The AMR-X-0 breadboard model (Figure 1) is made by 316L stainless steel, which limits the maximum gas temperature to about 1,000 K, for an expected ISP in the region of 50s with xenon. The purpose of this thruster is for concept validation and modeling verification. This concept is inspired by extensive previous work on high-temperature hydrogen resistojet done in 1970s[5-8]. However, the manufacturing and assembly of this devices was more complex, involving chemical vapor deposition of the thin tubular elements and the use of numerous EB welds to achieve a result similar to the monolithic AMR-X thruster.

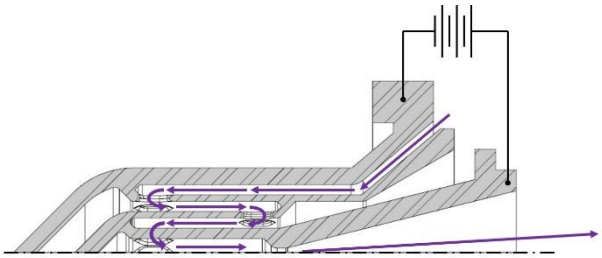

Figure 1. Axial-symmetric schematics of the AMR-X heat exchanger concept. The propellant flow path (purple) and the electrical interface are shown[9].

A. Gas dynamics

For the purpose of the test evaluation, the specific impulse generated by the resistojet can be approximated on the assumption of a one-dimensional adiabatic constant specific heat expansion through the nozzle, and applying a nozzle efficiency to account for incomplete expansion and divergence losses. This is described by Eq.(1), where $\eta_n = 0.9$ is the assumed nozzle efficiency, g_o=9.80665m/s the gravitational acceleration, c_p the constant-pressure specific heat of the propellant gas per unit mass and T_{in} the gas temperature at the inlet of the nozzle.

$$I_{sp} = \frac{\eta_n}{g_0}\sqrt{2c_p T_{in}} \tag{1}$$

The tests are operated at constant volumetric flow rate using a flow system developed to provide up to 3 ln/min of Xe with up to 4 bar absolute pressure, regulated by a pressure controller. Five flow rate set points have been selected to produce a thrust range from 10mN to 50mN. Pressure at the nozzle inlet can be estimated using the chocked flow Eq.(3), where R is the specific gas constant and γ the ratio of specific heats. Table 1 shows the estimated cold gas and hot gas specific impulse for Xe, the objective propellant, Ar, the tested propellant, and N2.

$$\dot{m} = \frac{F}{I_{sp} g_0} \tag{2}$$

$$p_t = \frac{\dot{m}\sqrt{T_{in}}}{A_t}\sqrt{\frac{R}{\gamma}}\left(\frac{\gamma+1}{2}\right)^{\frac{\gamma+1}{2(\gamma-1)}} \tag{3}$$

Table 1. Approximate specific impulse developed by a resistojet in the assumption of $\eta_n = 0.9$ for cold gas and hot gas modes.

Propellant	γ	c_p, $Jkg^{-1}K^{-1}$	ISP at T_{in} = 20°C	ISP at T_{in} = 500°C
Xe	1.67	158	28.0	45.4
Ar	1.67	520	50.7	82.3
N2	1.40	1024	71.1	115.5

B. Physical Description

Table 2 and Figure 2 show the AMR-X main components. The cold gas enters the thruster through a 1/8'' pipe, passing through the *thruster inflow* component, following an annular path, enveloping the thruster with relatively cold propellant up to the *nozzle spacer*. The flow continues flowing through the four recirculation channels created by the *heat exchanger*, finally reaching the converging-diverging nozzle. The set of four metal components listed in Table 2, are welded together, effectively creating a single component, through which both gas and electrical power can flow. Electrical power is supplied through positive and negative terminals, at the *casing* and at the *support* respectively, with the current flowing through the concentric tubular walls. By Eq.(4), the dissipated power is increased throughout smaller cross-sectional areas, closer to the inner concentric channels. The AMR-X is designed to develop highest gas temperature in the inner region and to obtain a maximum temperature at the inlet of the nozzle.

$$R = \rho \frac{l}{A} \tag{4}$$

The four heat exchanger concentric cylinder walls have a nominal thickness of 300µm, 150µm, 150µm and 300µm, from the innermost, which is 22 mm long. The nozzle has a throat diameter of 0.42 mm, a diverging half-angle of 14°, and inlet and outlet aspect ratios of 10 and 100 respectively.

Table 2. List of the main components of the AMR-X resistojet with materials and manufacturing process specified.

Component	Material	Manufacturing process
Heat Exchanger	316L SS	Selective Laser Melting
Thruster Inflow	316L SS	Selective Laser Melting
Casing	316L SS	Machined
Support	316L SS	Machined
Collar	Macor	Machined
Nozzle Spacer	Shapal	Machined
Ceramic thermal spacers	Macor	Machined

Figure 3 shows a fit assembly exercise on the AMR-X-0. An assembly involves two EB welds to join *heat exchanger – thruster inflow* (Figure 4, left) and *heat exchanger – thruster casing* (Figure 4, right). In addition, two TIG welds are performed to joining *thruster inflow – support* and *support* – inflow pipe.

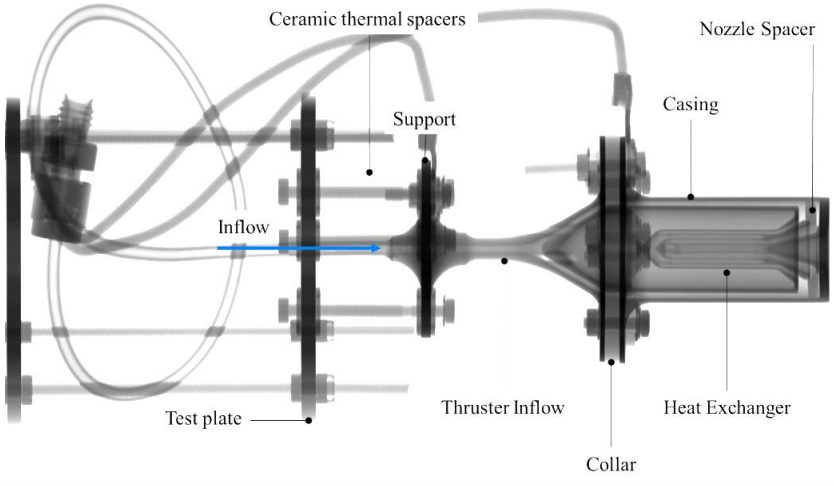

Figure 2. Radiograph of the AMR-X-0 assembly showing the main components and the recirculating flow path reaching the nozzle.

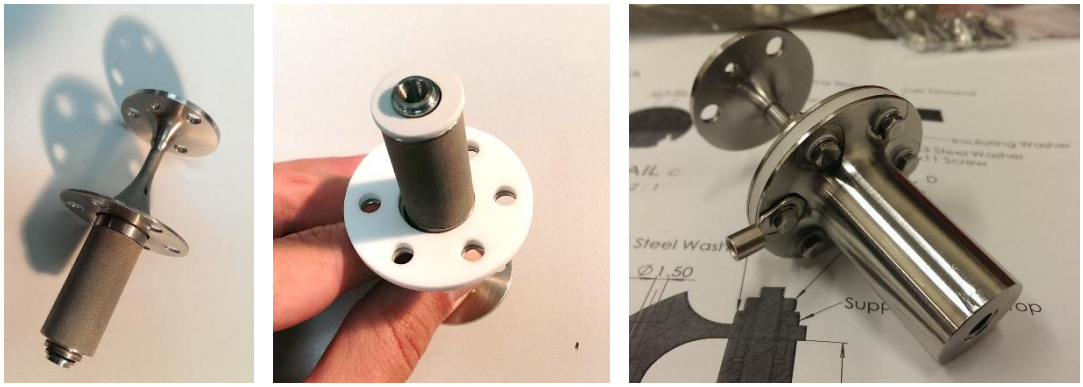

Figure 3. AMR-X-0 fit-assembly steps to establish proper tolerances prior EB welding.

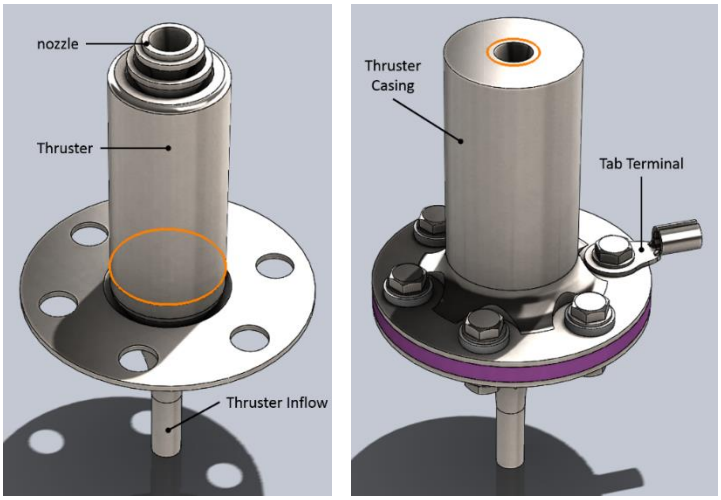

Figure 4. CAD model showing the position of the two EB welds performed on the AMR-X-0 assembly.

Unfortunately, prior testing a crack was observed on the Macor collar which forms a hermetic seal. From visual inspection it was not possible to determine whether the crack developed through the entire component. During tests, the thruster performed below expectation and a leak test was performed, confirming that a leak was located in the collar. After the test campaign, the resistojet assembly was inspected with a scatter-free radiograph using a 450kV source and a Collimated Linear Detector Array (CLDA) with 4 minutes of exposure in the mid-plane of the collar. The scan (Figure **5**, right) highlighted that the crack breaches the hermetic seal where the cold annular inflow is located (indicated by a red arrow). This is believed to be the source of the observed gas leak. Furthermore, the scan shows a second crack in the collar which did not influence the seal (top-right). Possible causes are excessive torque of 0.6Nm on the six M3 fasteners or handling during one of the preparation/assembly phases. Macor was selected for the breadboard model due to machinability and cost, however ceramics with much higher compressible strength are available and will be considered for the future test assemblies.

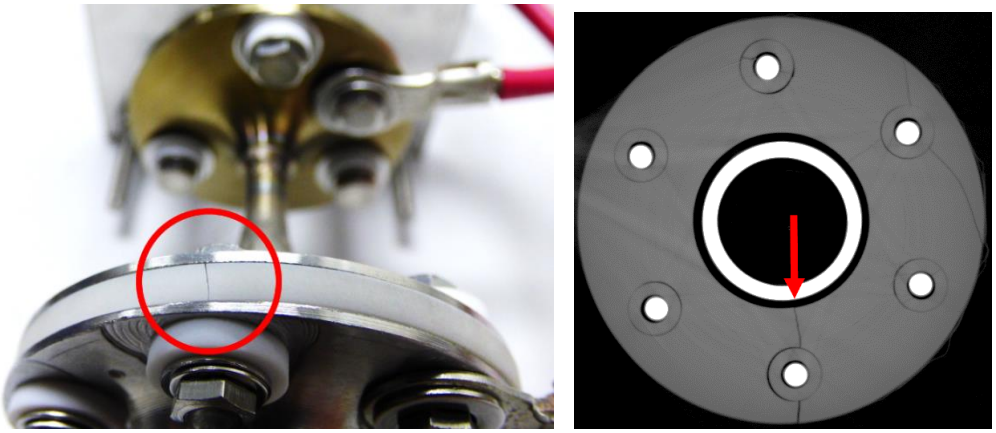

Figure 5. **Photo showing a crack developed in the ceramic collar.**

The AMR-X-0 design is the result of an extensive and iterative engineering process, in which the heat exchanger evolved through several generations. During this evolution, several design parameters and features were changed in an optimization process for SLM production, such as building angles, wall thickness, gap distances and fluidic channel geometry shape and size and support material. For the manufacturing verification process, more than 40 components have been produced by SLM[9]. The components are designed in Solidworks and exported in STL format then loaded in the SLM printer Concept Laser M2 Cusing. Once the printing process is completed, the excess powder is removed and the components are sectioned from the build plate by EDM wire-cut. Figure 6 shows a printing session where the *thruster* and *thruster inflow* have been produced (left) with a section view showing the two coupled components.

Figure 6. Thruster and Thruster Inflow as-printed components on the Concept Laser M2 Cusing base plate (left) and the two components assembled with a polished Thruster section.

High-resolution micro Computed Tomography (CT) is used as a tool for non-destructive inspection, since the concentric tubular heat exchanger of the thruster is entirely enclosed, preventing visual inspection. The CT volume data has been used to determine a surface mesh to perform coordinate measurement, nominal/actual comparison and wall thickness analysis[9]. This NDI tool has been vital for performing a successful design iteration process of the thruster.

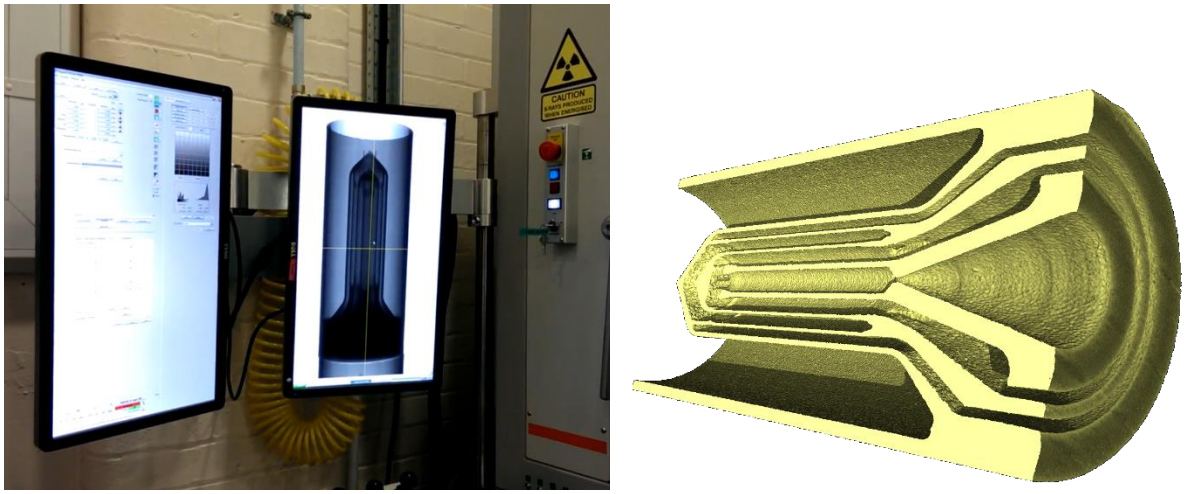

Figure 7. Radiograph of a Thruster prototype displayed at the µVIS X-Ray Imaging Centre (left) and micro-CT volumetric reconstruction of the AMR-X-0's heat exchanger.

A. Test set-up

The AMR-X breadboard model was tested at the David Fearn Electric Propulsion Laboratory at the University of Southampton (Figure 8). This facility has a main test chamber 4m long by 2m diameter, pumped by two cryopumps, 3 turbo-molecular pumps and 2 backing pumps, maintaining less than 5.5×10^{-5} mbar up to 30 sccm xenon and with a base pressure of $< 9 \times 10^{-8}$ mbar. The test rig is placed in the small hatch of the chamber, which can be isolated from the test chamber using a gate valve. This allows rapid test set up and preparation. The test results presented in this paper are performed in the main test chamber (Figure 9, right). The full set of instrumentation with measurement accuracy is shown in Table 3.

Thrust is directly measured with a Mettler-Toledo weighing module, with the resistojet mounted vertically through four M3 threaded bars (Figure 9, left). The AMR-X-0 assembly is mounted on an aluminum test plate. The 1/8'' stainless steel inflow pipe and the terminal cables are fixed on a second aluminum configuration plate, to avoid their thermal effects on the thrust measurement. From the resistojet to the feedthrough, the pipe is a flexible 1/8'' PFA. The resistojet is connected from the configuration plate to a levelled support jig 280mm on a side. In this way, any flexural force on the balance of the PFA pipe or of the terminal cables is kept to a minimum.

A Bronkhorst-based flow system provides either mass flow-controlled or pressure-controlled inflow to the thruster. The flow system is connected to both the Ar cylinder and to the chamber feedthrough with 1/4'' stainless steel hoses. The flow system was leak tested and when the flow system was evacuated to a pressure on the order of 10^{-2}mbar, after 6 days, the isolated pressure controller measured a pressure of 15mbar, which average to 1×10^{-1}mbar/hour leak in vacuum conditions.

The high-current DC power supply is used also for voltage and current monitoring. Thrust balance, flow system and power supply are connected to a workstation and controlled through the respective manufacture software. The thrust measurement is obtained simply by multiplying the measured weight by the gravity acceleration, $g_0 = 9.80665 \text{ms}^{-2}$.

Table 3. Summary of instrumentation used for the tests with measurement accuracy.

Instrument	Manufacturer	Type	Sym.	Range used	Accuracy
Thrust balance	Mattler Toledo	WMS404C	F	0 – 400g	0.1mg readability
MFC	Bronkhorst	F-201CV-5K0	$\dot{m}$	0.06 – 3 ln/min (Xe)	±0.5% RD plus ±0.1% FS
PC	Bronkhorst	P-602CV-21KA	p	0.12 – 6 bar (g)	± 0.5% FS
Power supply	Kikusui	PWX1500L	V	0 – 31.5V	± (0.5% of set + 0.05% of rating)
			I	0 – 157.5 A	± (0.5 % of set +0.1 % of rating)
Ohm-meter	Rhopoint Components Ltd	M210	R	1mΩ – 1.999Ω	± 0.1% of range
				0 – 1.4V	± 1mΩ zero offset

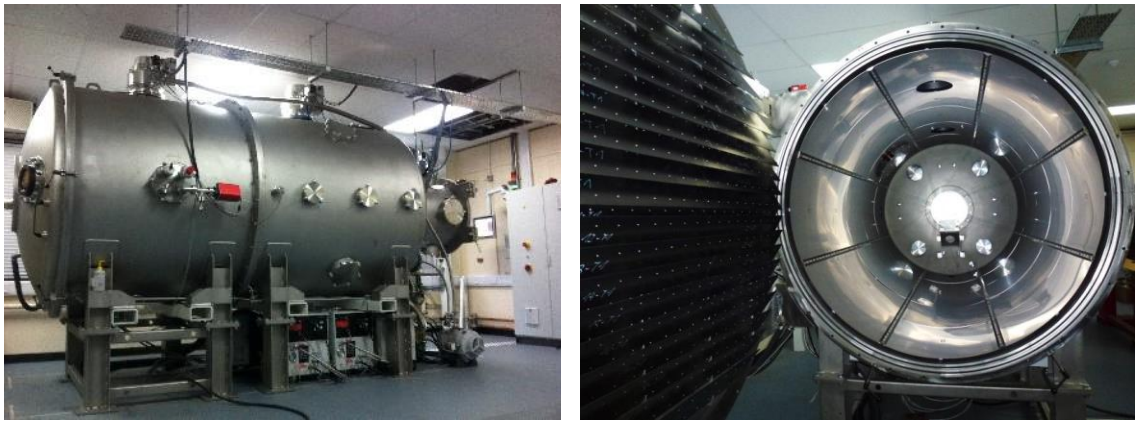

Figure 8. Overview of the David Fearn Electric Propulsion Laboratory at the University of Southampton (left) and the 4m long by 2m diameter test chamber section (right).

The balance calibration with thruster connections to the lateral support jig was checked with calibrated weights composed of four calibration weights of respectively, 20g, 10g and 2×2g giving 34.018g total. This gives up to the equivalent of 333.6 mN ±0.98mN based on stainless steel E2 class calibration weight precision, confirming the absence of any thrust drift due to the stiffness of the connections in the cold gas thrust mode. The measured weight it was monitored for a relatively long period to establish its accuracy.

The cold resistance from the resistojet terminals was 30mΩ, while at the feedthroughs the total measured resistance was 53mΩ due to the added resistance of the terminals harness, with the positive terminal harness of 12mΩ and the negative terminal harness of 10.5mΩ. The wire used for the connections is 10AWG copper wire, with 105 strands, resulting in approximately 3.2mΩ/m. Electrical connection between thruster and support jig, is achieved with a PVC 24A rated cable. The measurement drift at ambient temperature in air was within the balance readability. This was maintained during cold gas testes described in Section III. Thermal drift was however observed during heated operation due to thermal expansion of electrical supply lines, discussed later.

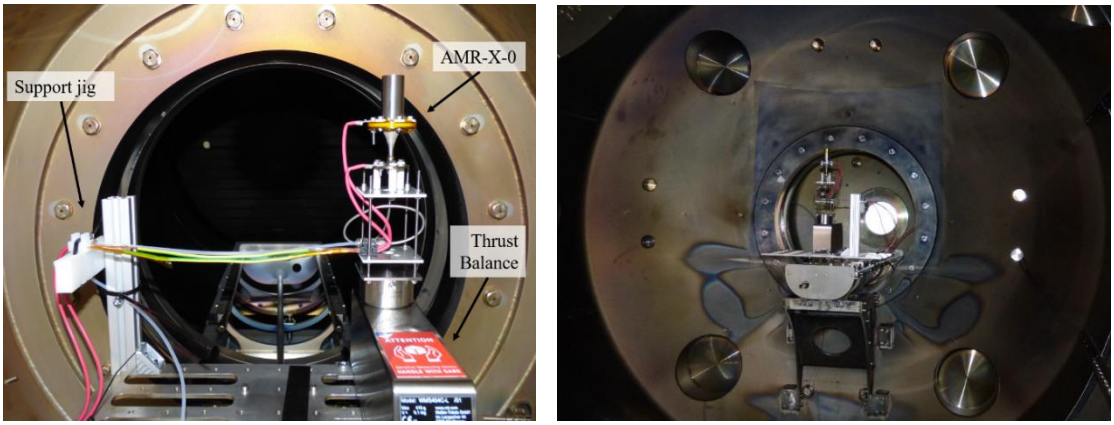

Figure 9. AMR-X-0 test rig placed in the small hatch (left), and in the 2m x 4.5m thermal vacuum test facility (right) at the David Fearn Electric Propulsion laboratory, University of Southampton.

III. Test results and discussion

The resistojet was tested with five different constant volumetric flow rates, and the heater was switched on in current limited mode at different electrical currents, as shown in Table 4. Flow rates were selected in order to produce a theoretical thrust from 10mN to 50mN. However, the previously discussed leak (Section B) must be taken into account for the ISP evaluation. It can be approximated considering that in cold mode, the specific impulse with Ar must be approximately 50.7s, using Eq.(1) and assuming a propellant temperature of 20°C at the inlet of the nozzle with a nozzle efficiency of 90%. This means that the loss in flow rate is proportional to the loss of thrust under cold conditions. The ISP has been estimated based on this hypothesis, using Eq.(2) since calculating ISP from the measured at the mass flow controller (MFC) would not be representative of the real flow rate reaching the converging-diverging nozzle.

The test procedure consisted in the following steps:

1. Pump down to vacuum chamber pressure of 1.8E-6 mbar with cryogenic pumps at <20K;
2. Operate at constant mass flow rate and reach a stable thrust level, while the chamber pressure reaches an equilibrium value;
3. If in hot gas mode, apply power in a current limited (CC) mode for the amount of time necessary to reach a maximum test thrust;
4. Switch off the electrical power, then the gas flow to assess baseline drift.

The maximum hot test thrust was conservatively selected as 150% of the cold gas case. To an increase in thrust at constant mass flow rate, corresponds an increase of specific impulse, Eq.(2), hence to an estimated maximum gas temperature from Eq.(1). As a result, the expected average nozzle inlet gas temperature would be of $T_{in} \approx 400$°C, for a corresponding ISP = 75.9s, with a leak correction. Table 4 shows the measured data for the five flow rates, which theoretically, without gas leak, should provide a thrust from 10mN to 50mN respectively. The cold gas tests 1, 5, 8, 10 and 11, provide a measured thrust of 74% to 57.6% of the expected thrust. It is believed that the flow rate loss is a consistent 25% in every case. In fact, the thrust is dependent on the chamber equilibrium pressure. As an example, with a flow rate of 0.678ln/min and an initial pressure of 3.1E-5mbar, the AMR-X-0 in cold mode develops 6.9mN, for a chamber pressure of 2.6E-3mbar and measured thrust of 69% of the expected thrust.

Table 4. Performance data of AMR-X-0 in vacuum with starting pressure of p_c = 1.8E-6 mbar and 20K of temperature.

Test #	MFC*, [ln/min]	Chamber pressure [p_c]	Thrust [mN]	ISP† [s]	Current [A]	Heating time‡ [s]
1	0.678	2.4E-4	7.4	50.6	0	NA
2	0.678	2.4E-4	11.1	75.9	15	240
3	0.678	2.4E-4	11.1	75.9	20	130
4	0.678	2.4E-4	11.1	75.9	25	83
5	1.356	6.0E-4	13.5	50.6	0	NA
6	1.356	6.0E-4	16	60.0	15	119
7	1.356	6.0E-4	16	60.0	20	79
8	2.032	9.5E-4	18.8	50.6	0	NA
9	2.032	9.5E-4	20.5	55.2	20	78
10	2.710	1.1E-3	23.9	50.6	0	NA
11	3.388	1.3E-3	28.8	50.6	0	NA

* Measured with the MFC, therefore not accounting for the gas leak.
† Estimated ISP.
‡ Heater ON after cold gas thrust peak reached.

Figure 10 shows the typical response of thrust after the heater is switched on after reaching constant thrust with a cold flow for Test 3 and Test 4 respectively. In both cases, the thrust is plotted along with the measured pressure at flow controller exit and with a subplot of the voltage-time heater characteristic measured at the power supply terminals. At the time the heater is switched on, thrust immediately increases, approaching almost a linear gradient as the heat exchanger increases in temperature. This shows that, at that specific flow rate, the heat exchanger was continuing to heat at a rapid rate before the imposed thrust limit was reached, indicating that at this power, the temperature, and thus ISP of the device could increase significantly. However, this would eventually exceed the material temperature limits of the current heat exchanger, while the purpose of this test is for concept validation and basic characterization. Although not observable in the graphs, the measured pressure increases of about 6-8% due to increasing pressure drop across the heat exchanger with increasing temperature.

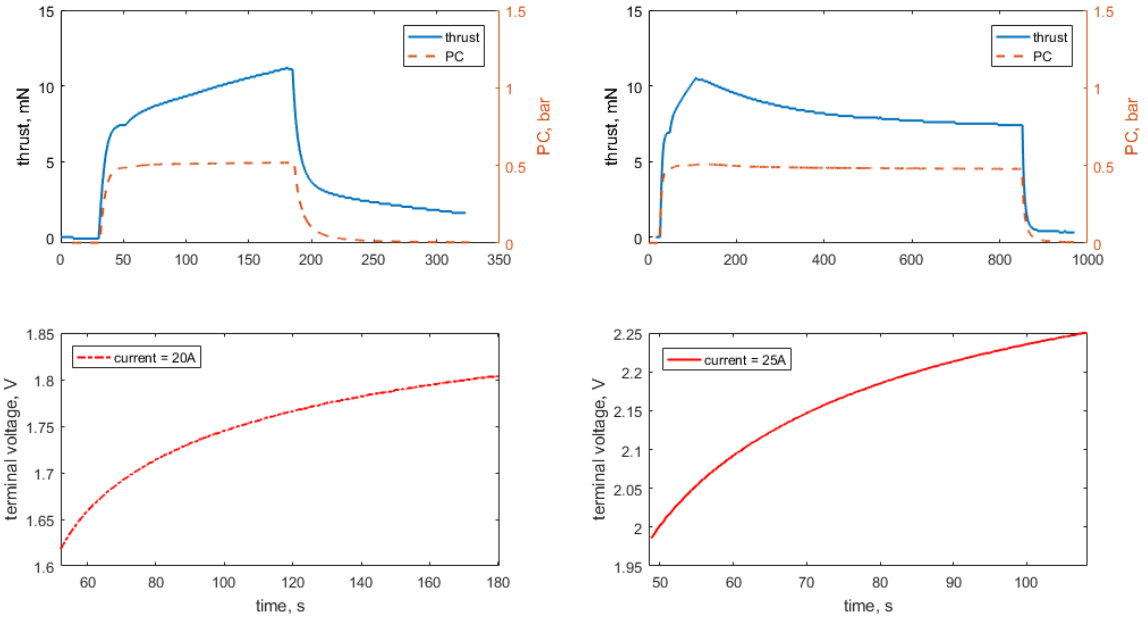

Figure 10. Effect of the gas heating to the thrust profile and to the operating voltage at a flow rate of 0.678ln/min with 20A and 25A of constant current. Test 3 (left) and Test 4 (right) are shown.

It should be mentioned, that while a thrust measurement drift was not observed in the cold gas tests, in the hot cases a significant drift was present as the device was switched off and flow rate was stopped. This is visible in both cases shown in Figure 10. The thrust measurement did eventually return to zero after tens of minutes. This behavior suggests that the terminal cables connecting the thruster to the support jig, are subjected to thermal expansion during hot mode, and influence the balance generating the described drift.

The resistojet electrical resistance is not directly measured during firing, however its cold resistance at the tab terminals is of 30mΩ. It is expected that the maximum resistance at tab terminals at 400°C should not exceed 45mΩ. Therefore, its maximum electrical power in test cases 2-4, with respective electrical currents of 15A, 20A and 25A should not exceed 10W, 18W and 28W respectively.

Figure 11 shows the voltage-time characteristic of the heater without propellant flow as a characterization exercise. In this cases, the voltage/time gradient is only slightly higher with respect to the flowing cases, highlighting that the AMR-X thruster can be safely pre-warmed up to reach the desired ISP in less time than that one indicated in Table 4.

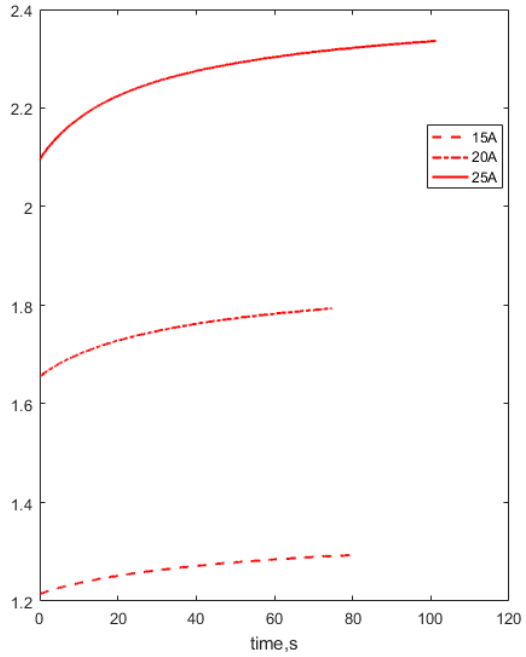

Figure 11. Terminal voltage measured at the power supply terminals with dry resistojet, such as in absence of propellant flow, at three different currents.

IV. Conclusions and Future Work

The AMR-X-0 has been tested with argon gas and characterized for a range of flow rates and discharge currents. The preliminary tests here show for the first time that the concept of the additively manufactured concentric tubular heat exchanger with integrate nozzle is a feasible and concept.

Tests have been performed with constant flow rates, and it has been demonstrated that for a range of electrical powers that the thrust, hence the specific impulse, was improved up to 50%, determining that the stainless steel AMR-X-0 prototype can readily develop a hot gas temperature in the region of 400°C. However, the breadboard model in analysis suffered from a gas leak located in the ceramic insulator, caused by a crack connecting the flow path with the ambient. A backup thruster AMR-X-1, which is currently under manufacturing, will be soon tested.

The resistojet has been tested with argon. The future involves further characterization of the stainless steel prototype with Xe gas, for which it is designed. A development program is currently ongoing to manufacture the concept with the same processes in refractory metals, which will enable specific impulse above 80s with Xe.

A multiphysics model of the AMR-X thruster has been developed in COMSOL Multiphysics. This model, which has been used for analysis of experimental results available in literature[10], was been used as a design tool to meet the performance requirements generated by industry. This model will be compared with the present and future test results to be validated and provide a better insight of the thruster behavior and ISP in particular. In the upcoming test campaign, the resistojet will be evaluated in different modes: constant flow rate, constant pressure, pre-heating of the heat exchanger to achieve rapidly high performance, and will also be tested with the complete set of components, which includes radiation shields and thermal insulation with more detailed diagnostics.

Acknowledgments

Part of this research was funded by the Doctoral Training Partnership through the Engineering and Physical Sciences Research Council (EPSRC) [grant number EP/M50662X/1]. This work was also supported by Innovate UK in the CEOI-ST National Space Technology Programme (NSTP-2) in partnership with Surrey Satellite Technology Limited as an end-user of the technology of the High Performance Xenon Resistojet. The project is also currently supported by the UK Space Agency in the framework of the Refractory Additive Layer Manufacturing for Commercial Space Applications (RADICAL) project. The authors are also grateful for help from the μ-VIS X-Ray Imaging Centre for X-ray Tomography at the University of Southampton.

References

[1]Gibbon, D., I. Coxhill, and M. Drube, *The Design, Build Test and In-Orbit Performance of the Giove-A Propulsion System*, in *5th International Spacecraft Propulsion Conference*. 2008: Crete.

[2]Coxhill, I.G. and D. Gibbon, *A Xenon Resistojet Propulsion System for Microsatellites*, in *41st AIAA/ASME/SAE/ASEE Joint Propulsion Conference & Exhibit*. 2005: 10-13 July.

[3]Nicolini, D., et al., *Xenon Resistojets as Secondary Propulsion on EP Spacecrafts and Performance Result of Resistojet Using Xenon*, in *28th International Electric Propulsion Conference*. 2003: Toulouse, France.

[4]Grubisic, A.N. and S.B. Gabriel, *Assessment of the T5 and T6 Hollow Cathodes as Reaction Control Thrusters.* Journal of Propulsion and Power, 2016(null): p. 1-11.

[5]Donovan, J.A., W.T. Lord, and P.J. Sherwood, *Fabrication and Preliminary Testing of a 3kW Hydrogen Resistojet*, in *The AIAA 9th Electric Propulsion Conference*. 1972.

[6]Donovan, J. and W. Lord, *Performance Testing of a 3kW Hydrogen Resistojet*. 1973, DTIC Document.

[7]Sherwood, P., *Construction of a High Performance Resistojet for Satellite Propulsion*. 1978, DTIC Document.

[8]Page, R.J. and R.A. Short, *Design of High-Performance Resistojets for Advanced Spacecraft*, in *9th Aerospace Sciences Meeting-Separate Papers - AIAA*, A.R. Technology, Editor. 1971. p. No.71-195.

[9]Romei, F., A.N. Grubišić, and D. Gibbon, *Manufacturing of a high-temperature resistojet heat exchanger by selective laser melting.* Acta Astronautica, 2017. **138**: p. 356-368.

[10]Romei, F. *Multiphysics model validation of resistojets with concentric tubular heat exchanger*. in *7th European Conference for Aeronautics and Space Science (EUCASS)*. 2017.